Available online at www.sciencedirect.com
SCIENCE DIRECT®
Journal of Power Sources 134 (2004) 277–292
JOURNAL OF POWER SOURCES
www.elsevier.com/locate/jpowsour

Extended Kalman filtering for battery management systems of LiPB-based HEV battery packs Part 3. State and parameter estimation

Gregory L. Plett*,[1]

Department of Electrical and Computer Engineering, University of Colorado at Colorado Springs, 1420 Austin Bluffs Parkway, P.O. Box 7150, Colorado Springs, CO 80933-7150, USA

Received 27 January 2004; accepted 26 February 2004

Available online 28 May 2004

Abstract

Battery management systems in hybrid-electric-vehicle battery packs must estimate values descriptive of the pack's present operating condition. These include: battery state-of-charge, power fade, capacity fade, and instantaneous available power. The estimation mechanism must adapt to changing cell characteristics as cells age and therefore provide accurate estimates over the lifetime of the pack.

In a series of three papers, we propose methods, based on extended Kalman filtering (EKF), that are able to accomplish these goals for a lithium ion polymer battery pack. We expect that they will also work well on other battery chemistries. These papers cover the required mathematical background, cell modeling and system identification requirements, and the final solution, together with results.

This third paper concludes the series by presenting five additional applications where either an EKF or results from EKF may be used in typical BMS algorithms: initializing state estimates after the vehicle has been idle for some time; estimating state-of-charge with dynamic error bounds on the estimate; estimating pack available dis/charge power; tracking changing pack parameters (including power fade and capacity fade) as the pack ages, and therefore providing a quantitative estimate of state-of-health; and determining which cells must be equalized. Results from pack tests are presented.

Keywords: Battery management system (BMS); Hybrid-electric-vehicle (HEV); Extended Kalman filter (EKF); State-of-charge (SOC); State-of-health (SOH); Lithium-ion polymer battery (LiPB)

1. Introduction

This paper is the third in a series of three that describe advanced algorithms for a battery management system (BMS) for hybrid-electric-vehicle (HEV) application. This BMS is able to estimate battery state-of-charge (SOC), power fade, capacity fade and instantaneous available power, and is able to adapt to changing cell characteristics over time as the cells in the battery pack age. The algorithms have been implemented on a lithium-ion polymer battery (LiPB) pack, but we expect them to work well for other battery chemistries.

The method we use to estimate these quantities is based on Kalman filter theory. Kalman filters are an intelligent—and sometimes optimal—means for estimating the *state* of a dynamic system. By employing a mathematical model of our battery system that includes the unknown quantities in the model state, we may use the Kalman filter to estimate them. An additional benefit of the Kalman filter is that it automatically provides dynamic error bounds on these estimates. We exploit this fact to give aggressive performance from our battery pack, without fear of causing damage.

We focus on the HEV application, although we believe that the results should generalize to other less strenuous battery uses. To summarize, important aspects of state and parameter estimation required in an HEV application are:

- The estimates must be accurate for all operating conditions. These include: very high rates (many papers consider rates up to about ±3C for portable electronic applications; we need to consider rates up to and exceeding

* Tel.: +1-719-262-3468; fax: +1-719-262-3589.
E-mail addresses: gplett@compactpower.com, glp@eas.uccs.edu (G.L. Plett).
URL: http://mocha-java.uccs.edu.
[1] The author is also consultant to Compact Power Inc., Monument, CO 80132, USA. Tel.: +1-719-488-1600x134; fax: +1-719-487-9485.

0378-7753/$ – see front matter © 2004 Elsevier B.V. All rights reserved.
doi:10.1016/j.jpowsour.2004.02.033

±20C), temperature variation in the automotive range −30 to 50 °C, very dynamic rate profiles (unlike the more benign portable electronic and battery electric vehicle application). Charging (by the engine providing extra power, or by regenerative braking) must be accounted for.
- We require noninvasive methods using only readily available signals. This requirement is imposed by the HEV environment where the BMS has no direct control over current and voltage experienced by the battery pack—this is in the domain of the vehicle controller and inverter. This requirement implies that we must rely on such measurements as instantaneous cell terminal voltage, cell current and cell external temperature.
- Our cell chemistry also limits the range of approaches we might consider. Techniques specific to lead-acid chemistries, for example, are not appropriate for LiPB cells.

Methods based on extended Kalman filtering meet these needs very well.

The first paper in the series introduces the problem [1]. It describes the HEV environment and the requirements specifications for a BMS. The remainder of the paper is a quick review of the Kalman filter theory necessary to grasp the content of the remaining papers; additionally, a nonlinear extension called the "extended Kalman filter" (EKF) is discussed.

The second paper describes some mathematical cell models that may be used with this method [2]. It also gives an overview of other modeling methods in the literature and shows how an EKF may be used to adaptively identify unknown parameters in a cell model, in real time, given cell voltage, current, and temperature measurements.

This third paper outlines the primary applications of EKF to the estimation requirements for battery management. Namely, how one can estimate SOC, available power, and characteristics of aging cells. In particular, we might wish to estimate *power fade* and *capacity fade* to somehow quantify cell *state-of-health* (SOH). Power fade refers to the phenomenon of increasing cell electrical resistance as the cell ages. This increasing resistance causes the power that can be sourced/sunk by the cell to drop. Capacity fade refers to the phenomenon of decreasing cell total capacity as the cell ages. The literature reports various different approaches to estimating SOH (primarily capacity fade). These include:

- The *discharge test*, which completely discharges a fully charged cell in order to determine its total capacity [3]. This test interrupts system function and wastes battery energy, so is not applicable to the HEV BMS environment.
- *Chemistry-dependent methods*, such as measuring the level of plate corrosion, electrolyte density or "*coup de fouet*" for lead-acid batteries [4–7]. The methods presented here are general.
- *Ohmic tests*, such as resistance, conductance or impedance tests, perhaps combined with fuzzy-logic algorithms [6,8–22]. These methods require making measurements we cannot make for our application, as we may not inject signals into the battery pack.
- *Partial discharge*, or other methods that compare cell-under-test to a good cell or model of a good cell [3,23–26]. Extended Kalman filtering is a rigorous approach using this idea.

These methods are also limited by their specificity. For example, cell resistance and capacity are only two of a number of time-varying cell parameters we might wish to estimate. In this paper we will show that EKF may be used to estimate all cell parameters.

This paper proceeds to describe applications of EKF to BMS. First, EKF for SOC estimation is presented, secondly, dynamic maximum power estimation relying on the EKF state estimate is outlined. Thirdly, dual EKF for state and parameter estimation is introduced. Finally, an equalization calculation using dual EKF derived parameters and state estimates is derived. In all sections, relevant results are presented.

2. Applications I and II: initialization and SOC estimation

The principal focus of this paper is to present applications of the EKF algorithm (explained in [1] and summarized in Table 1 for clarity), combined with cell models (identified in [2] and summarized in Table 2), to battery management system functions. The first application we explore is that of estimating cell SOC in a dynamic environment.

As we have seen, EKF is a method for system state estimation in real time. In our application, the algorithm compares measured cell terminal voltage, under load, with the value predicted by a cell model. The difference between these

Table 1
Summary of the nonlinear extended Kalman filter from [27]

Nonlinear state-space model[a]

$$x_{k+1} = f(x_k, u_k) + w_k$$
$$y_k = g(x_k, u_k) + v_k$$

Definitions

$$A_{k-1} = \left.\frac{\partial f(x_{k-1}, u_{k-1})}{\partial x_{k-1}}\right|_{x_{k-1}=\hat{x}_{k-1}^+}, \quad C_k = \left.\frac{\partial g(x_k, u_k)}{\partial x_k}\right|_{x_k=\hat{x}_k^-}$$

Initialization

For $k = 0$, set

$$\hat{x}_0^+ = \mathbb{E}[x_0]$$
$$\Sigma_{\tilde{x},0}^+ = \mathbb{E}[(x_0 - \hat{x}_0^+)(x_0 - \hat{x}_0^+)^{\mathrm{T}}]$$

Computation

For $k = 1, 2, \ldots$ compute

State estimate time update: $\hat{x}_k^- = f(\hat{x}_{k-1}^+, u_{k-1})$

Error covariance time update: $\Sigma_{\tilde{x},k}^- = A_{k-1}\Sigma_{\tilde{x},k-1}^+ A_{k-1}^{\mathrm{T}} + \Sigma_w$

Kalman gain matrix: $L_k = \Sigma_{\tilde{x},k}^- C_k^{\mathrm{T}}[C_k \Sigma_{\tilde{x},k}^- C_k^{\mathrm{T}} + \Sigma_v]^{-1}$

State estimate measurement update: $\hat{x}_k^+ = \hat{x}_k^- + L_k[y_k - g(\hat{x}_k^-, u_k)]$

Error covariance measurement update: $\Sigma_{\tilde{x},k}^+ = (I - L_k C_k)\Sigma_{\tilde{x},k}^-$

[a] w_k and v_k are independent, zero-mean, Gaussian noise processes of covariance matrices Σ_w and Σ_v, respectively.

Table 2
Summary of cell models from [2]

Combined model: note that K_0 through K_4 are constants to fit the model

$$z_{k+1} = z_k - \left(\frac{\eta_i \Delta t}{C}\right) i_k$$
$$y_k = K_0 - Ri_k - \frac{K_1}{z_k} - K_2 z_k + K_3 \ln(z_k) + K_4 \ln(1 - z_k)$$

Simple model: note that OCV$(\cdot)$ is open-circuit-voltage

$$z_{k+1} = z_k - \left(\frac{\eta_i \Delta t}{C}\right) i_k$$
$$y_k = \mathrm{OCV}(z_k) - Ri_k$$

Zero-state hysteresis model: note that $M(\cdot)$ is maximum hysteresis

$$z_{k+1} = z_k - \left(\frac{\eta_i \Delta t}{C}\right) i_k$$
$$y_k = \mathrm{OCV}(z_k) - s_k M(z_k) - Ri_k$$

Single-state hysteresis model: note that $F(i_k) = \exp\left(-\left|\frac{\eta_i i_k \gamma \Delta t}{C}\right|\right)$, γ is hysteresis rate constant, $M(\cdot,\cdot)$ is maximum hysteresis

$$\begin{bmatrix} h_{k+1} \\ z_{k+1} \end{bmatrix} = \begin{bmatrix} F(i_k) & 0 \\ 0 & 1 \end{bmatrix} \begin{bmatrix} h_k \\ z_k \end{bmatrix} + \begin{bmatrix} 0 & (1 - F(i_k)) \\ -\frac{\eta_i \Delta t}{C} & 0 \end{bmatrix} \begin{bmatrix} i_k \\ M(z, \dot{z}) \end{bmatrix}$$
$$y_k = \mathrm{OCV}(z_k) - Ri_k + h_k$$

Enhanced self-correcting (ESC) model: α are filter-pole locations

$$\begin{bmatrix} f_{k+1} \\ h_{k+1} \\ z_{k+1} \end{bmatrix} = \begin{bmatrix} \mathrm{diag}(\alpha) & 0 & 0 \\ 0 & F(i_k) & 0 \\ 0 & 0 & 1 \end{bmatrix} \begin{bmatrix} f_k \\ h_k \\ z_k \end{bmatrix} + \begin{bmatrix} 1 & 0 \\ 0 & (1 - F(i_k)) \\ -\frac{\eta_i \Delta t}{C} & 0 \end{bmatrix} \begin{bmatrix} i_k \\ M(z, \dot{z}) \end{bmatrix}$$
$$y_k = \mathrm{OCV}(z_k) - Ri_k + h_k + Gf_k$$

z_k is SOC, η_i the Coulombic efficiency, i_k the current, y_k the predicted cell voltage, Δt the sampling interval, C the nominal capacity, R the cell resistance.

quantities is used to adapt the state of the cell model so that the model output more closely matches the measured cell voltage, and the model state more closely matches the real quantities it estimates. By enforcing that SOC be a member of the model state, as is the case with all model structures in Table 2, we directly estimate *both* SOC and the uncertainty (error bounds) of the estimate. Note that since we use EKF versus KF, we are able to use precise nonlinear cell models in our SOC estimator, improving the SOC estimation accuracy.

Before presenting some results, we first discuss how the algorithm's state and uncertainties might be initialized when the vehicle is started. That is, how we might propagate $\hat{z}_k$ and $\Sigma_{\tilde{z},k}$ across the interval between key-off and key-on. For this, we employ the SOC estimate and $\Sigma_{\tilde{z}}$ values saved when the vehicle was previously turned off, the period of time the vehicle was off, and a very simple cell self-discharge model. Our empirical data indicates that SOC decays approximately exponentially due to self-discharge, allowing us to create a continuous-time state-space model for self-discharge. Let $z(t)$ be the state-of-charge as a function of self-discharge time. Then

$$z(t) = -\phi z(t) + w(t)$$
$$y(t) = \mathrm{OCV}(z(t)) + v(t),$$

where ϕ is the rate of SOC decay, w is small and v depends on the period since key-off. We can form a discrete-time version of this model. Let t_{off} be the period that the vehicle is off. Then,

$$z_{k+1} = \mathrm{e}^{-\phi t_{\mathrm{off}}} z_k + w_k$$
$$y_k = \mathrm{OCV}(z_k) + v_k.$$

Applying the EKF to this system estimates SOC and $\Sigma_{\tilde{z}}$. Filter states are initialized to zero with $\Sigma_{\tilde{f}}$ initialized to small values. The hysteresis state and covariance are unchanged by power-down.

In order to demonstrate the performance of EKF in estimating SOC with the various cell models, we need to first discuss some cell tests. Data was gathered from a prototype hand-made LiPB cell comprising a $LiMn_2O_4$ cathode, an artificial graphite anode, and designed for high-power applications, having a nominal capacity of 7.5 Ah and a nominal voltage of 3.8 V. For the tests, we used a Tenney thermal chamber set at 25 °C and an Arbin BT2000 cell cycler. Each channel of the Arbin was capable of 20 A current, and 10 channels were connected in parallel to achieve currents of up to 200 A. The cycler's voltage measurement accuracy was ±5 mV and its current measurement accuracy was ±200 mA. Two different cell tests were performed:

- *Pulsed-current test*: The first test comprised a sequence of discharge pulses and rests followed by a sequence of charge pulses and rests. This test was designed to explore the cell response to very high and very low currents

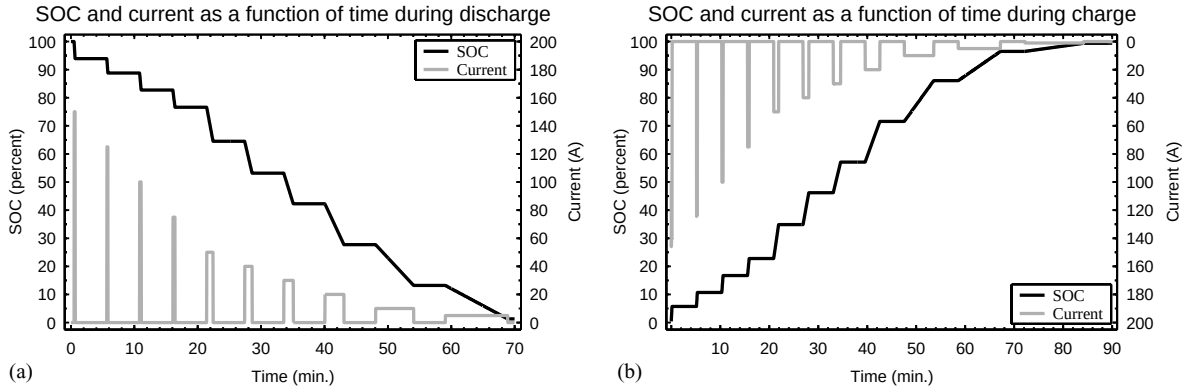

Fig. 1. Plots showing SOC versus time and rate versus time for pulsed-current cell tests. Discharge portion of test is shown in (a); charge portion of test is shown in (b). Dark line is SOC, gray line is current.

where dynamics were minimally excited. The cell was initially fully charged. Discharge current pulses from 150 A down to 1 A were used. Charge pulses from 150 A down to 1 A were used. The current and SOC profiles for this test are shown in Fig. 1(a) and (b). Frame (a) shows the discharge portion of the test and frame (b) shows the charge portion of the test. Data points (including voltage, current, ampere-hours discharged and ampere-hours charged) were collected once per second.

- *UDDS dynamic test*: The second test was a sequence of fifteen "urban dynamometer driving schedule" (UDDS) cycles, separated by 40 A discharge pulses and 5-min rests, and spread over the 90–10% SOC range. This test was designed to excite all cell dynamics in a fashion similar to what would be experienced in an HEV battery pack. The rate profile was generated from a Matlab ADVISOR [28] simulation for a vehicle roughly twice the size of the Honda Insight, and is shown in Fig. 2(a) for one UDDS cycle. Fig. 2(b) shows the SOC trace for the entire test. We see that SOC increases by about 5% during each UDDS cycle, but is brought down about 10% by the 40 A discharge between cycles. The entire operating range for these cells (10% SOC to 90% SOC) is excited during the cell test. Data points were collected once per second for this test as well.

In all cases, "true" SOC was calculated from the Arbin data log using Coulomb counting on measured data. Note that the "true" SOC is only approximately accurate since current sensor error accumulated over time causes any estimate computed using Coulomb counting to eventually diverge.

Results using the EKF to estimate SOC for the pulsed-current test—using the six cell models—are shown in Figs. 3–5. Results for the UDDS tests are shown in Fig. 6. Rather than plotting both "true" and estimated SOC for purpose of evaluating the effectiveness of the EKF, we instead plot estimation error calculated as "true" value minus estimated value. This amplifies the detail that can be seen in the plots. Also shown are the three-sigma error bounds (the confidence region of the estimate) using EKF. In all plots, the thick black line is the estimation error, and the thin gray lines delineate the confidence region of the estimate. Ideally, the estimation error is zero and the confidence region always includes the value zero.

We first discuss the results of the pulsed-current tests. Fig. 3 shows the results of EKF SOC estimation for all models with only SOC as a state, when the SOC state was correctly initialized to 100%. Results for the combined model are shown in frames (a) and (d); results for the simple model are shown in frames (b) and (e); and results for the zero-state hysteresis model are shown in frames (c) and (f). The left

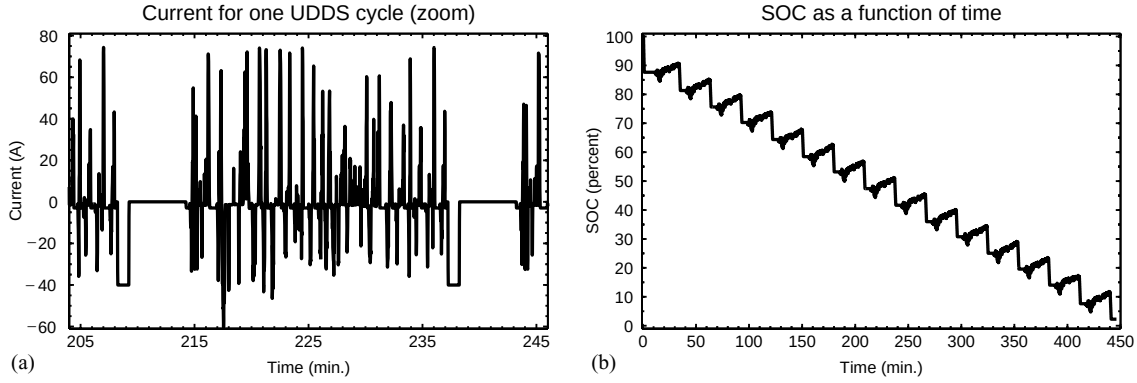

Fig. 2. Plots showing SOC versus time and rate versus time for UDDS cell tests. Rate for one UDDS cycle is shown in (a); SOC for the entire test is shown in (b).

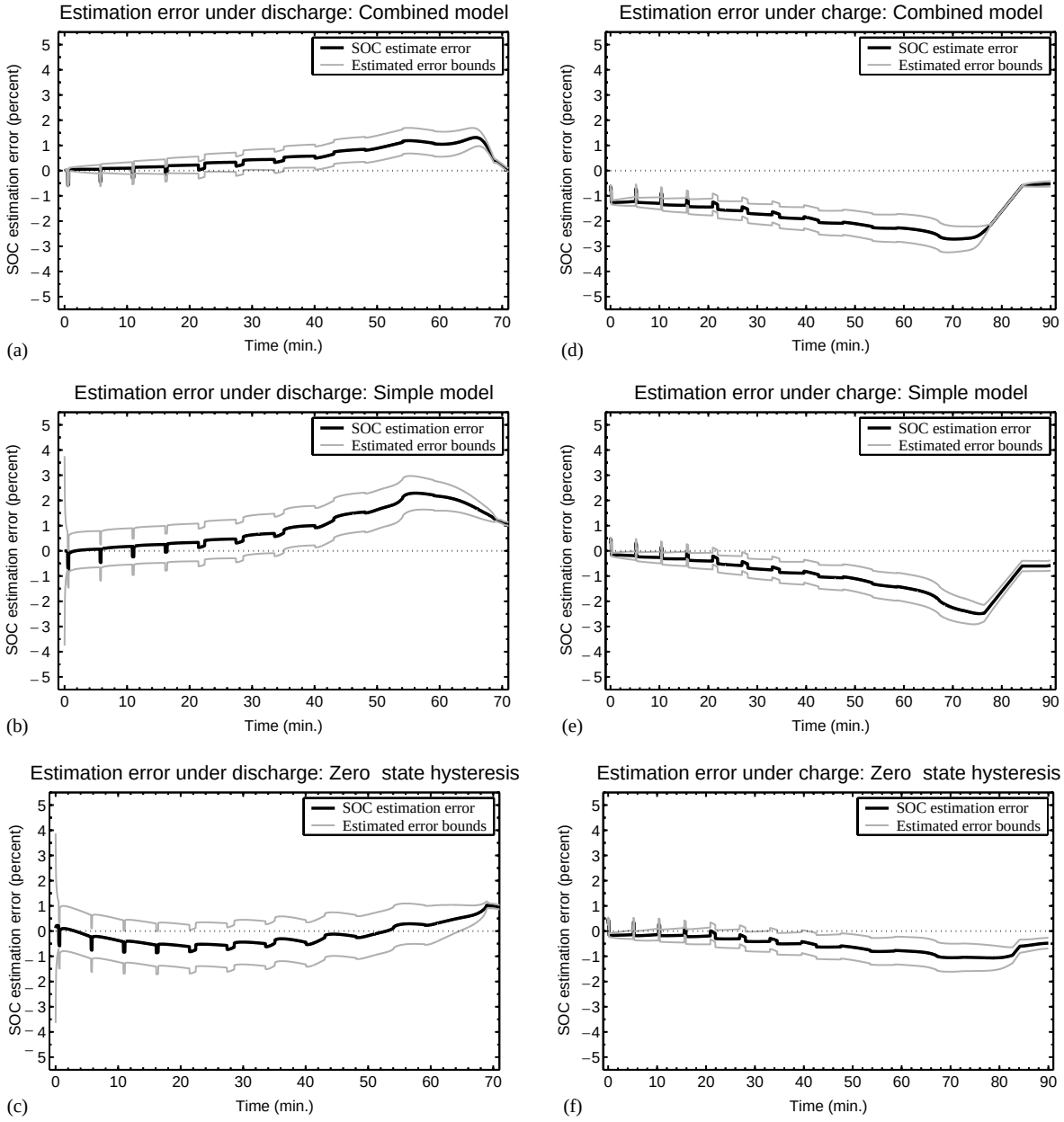

Fig. 3. Results of SOC estimation using models with only SOC as a state for the pulsed-current cell tests. Discharge portion of test is shown in (a)–(c); charge portion of test is shown in (d)–(f). The dark line is the true cell SOC minus the estimated SOC, and the thin gray lines demarcate the error bounds on the estimate.

column shows results for the discharge portion of the test, and the right column shows results for the charge portion of the test. Since the EKF was correctly initialized in all cases, the estimation error starts at zero. For both the combined and simple models, the error slowly diverges away from zero for much of the discharge segment; the zero-state hysteresis model does a better job. As the discharge portion of the test concludes, the estimation error of all three models drops to about 1% or better. One reason for the divergence of the SOC estimate for the simpler models is that the OCV curve for these cells is extremely flat over much of the SOC range. Voltage measurement error of $\pm 5\,\text{mV}$ can account for as much as 6.5% SOC error if used alone, and is worst around the level of SOC = 60%. The simpler models do not sufficiently account for the dynamics of the cell, and rely most heavily on OCV. In these cells, as SOC approaches zero, the OCV curve drops precipitously to 3.0 V, so is a much more accurate estimator of SOC. The effect of this in the EKF SOC estimators is that the estimation error improves considerably toward the end of the discharge. (All models using OCV as part of the output equation converge to an error of about 1%, which indicates that the empirical OCV versus SOC relationship used by the models may be slightly incorrect.)

The discharge portion of the pulsed-current test that is shown in the figures draws the cell's true SOC down to about

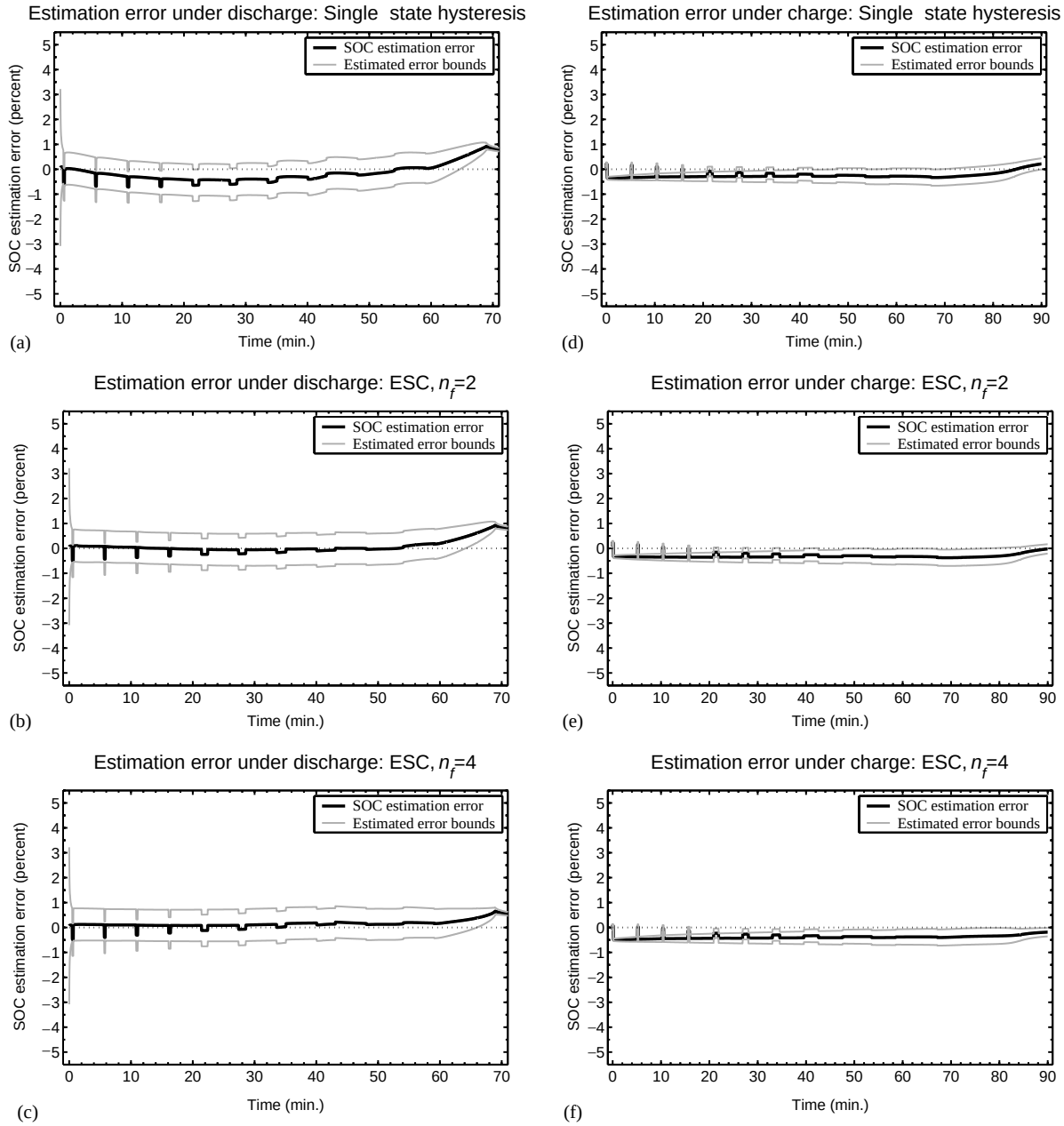

Fig. 4. Results of SOC estimation using models with multiple states for the pulsed-current cell tests. Discharge portion of test is shown in (a)–(c); charge portion of test is shown in (d)–(f). The black line is the true cell SOC minus the estimated cell SOC, and the thin gray lines demarcate the error bounds on the estimate.

1%. Not shown is a subsequent long slow discharge down to 0%. The charge portion of the pulsed-current test immediately follows this long discharge. In the EKF validation tests, the discharge portion(s) and charge portion are not considered separately, but as a unit; that is, the EKF is initialized before the discharge, and then run for the entire 160+ minutes without re-initialization between the discharge and charge portions. This explains why the SOC estimation error is not initially zero in all of the charge portions of the test. The combined model starts with the worst estimation error as it does not use true OCV versus SOC in its output equation, but only an approximation. This approximation is worst around 0%. Again, estimation error for the simpler models diverges over a large portion of the test, only converging toward zero as SOC approaches 100% where the OCV versus SOC curve is no longer flat. The zero-state hysteresis model is somewhat better than the other two models in this respect.

In all of the tests discussed so far, the confidence interval of the estimation error is also poor. The EKF "thinks" that its estimate is much better than it actually is. This is not the fault of the EKF method itself, but rather of the cell model being used. If the cell model were accurate, the error bounds would also be accurate. The inaccuracy of the simpler cell models leads to over-confidence in the estimate.

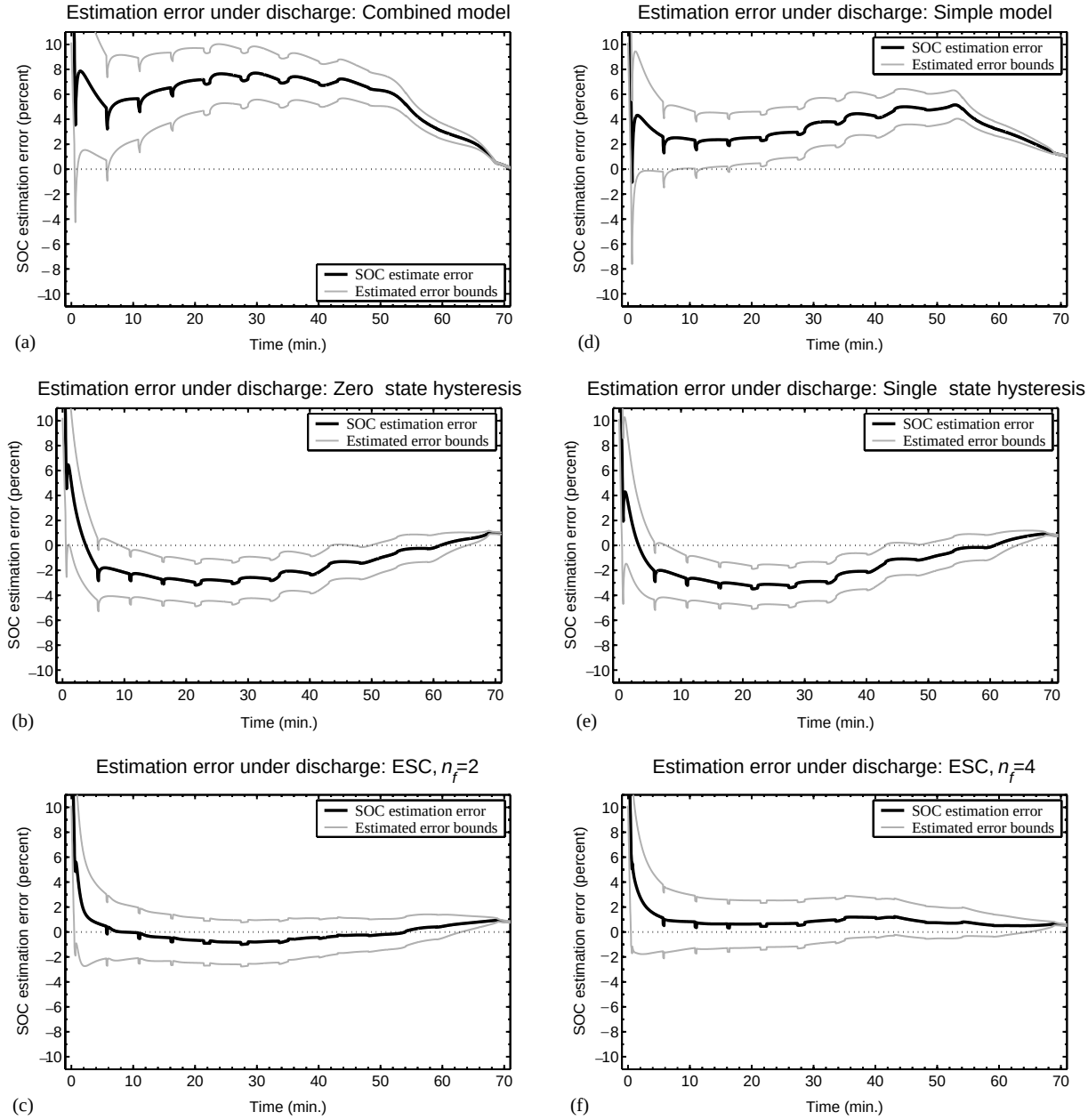

Fig. 5. Results of SOC estimation where the initial estimator state was set to 80% while the true initial state was 100%. The dark line is the true cell SOC minus the estimated SOC, and the thin gray lines demarcate the error bounds on the estimate.

Fig. 4 shows the results of EKF SOC estimation for models with multiple states, when the SOC state was correctly initialized to 100% (filter and hysteresis states were initialized to zero). Results for the single-state hysteresis model are shown in frames (a) and (d); results for the ESC model using two filter states are shown in frames (b) and (e); and results for the ESC model using four filter states are shown in frames (c) and (f). In all cases, estimation error is much improved over the models with only SOC as a state. We again see that error converges to about 1% at the end of discharge, most likely due to an imprecise OCV versus SOC relationship. We also see that the EKF confidence region much more accurately describes the true confidence of the estimate.

From these figures alone, it would be difficult to definitively determine the "best" model to be used in a BMS. We now present some additional results that help with the decision, based on considerations of robustness. In practice, the Kalman filter would be initialized with a priori state estimates when the vehicle is turned on (based on OCV readings and a look-up table, plus self-discharge rate data from the cell model and the prior SOC when the vehicle was turned off). In the results we have seen, the EKFs were initialized using the correct SOC of 100%. Correct initialization is not guaranteed in practice, especially if the SOC is in the neighborhood of 50% (around the flat portion of the OCV versus SOC curve), and if the cells have not relaxed from recent ac-

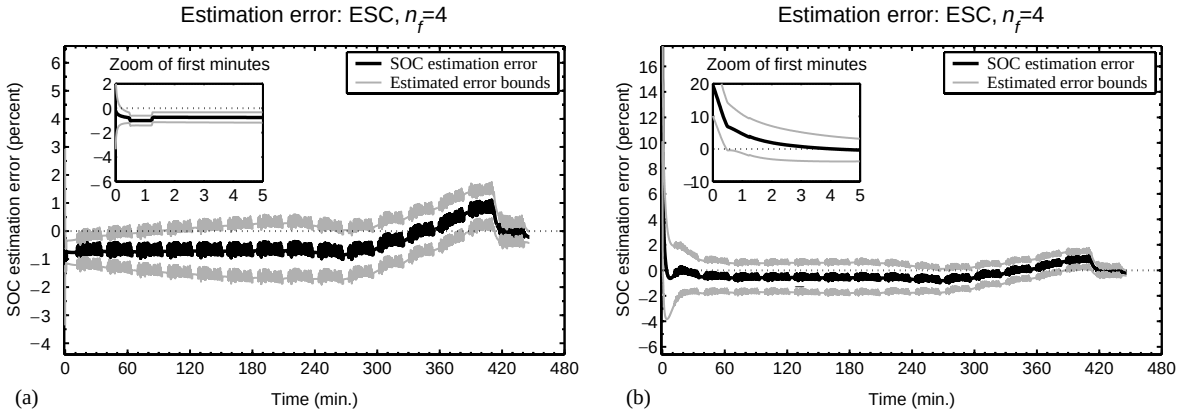

Fig. 6. Results of SOC estimation on UDDS data. In (a) the initial estimator state was correctly set to 100%; in (b) the initial estimator state was set to 80% while the true initial SOC was 100%. Dark line is SOC estimation error, gray lines demarcate the error bounds on the estimate.

tivity (For example, the automobile might have been turned off for only a few minutes while the driver filled the gas tank or purchased a cup of coffee.) Fig. 5 show examples of EKF SOC estimation for the pulsed-current data set (discharge portion only for purpose of brevity) where the filter SOC state was incorrectly initialized to 80% instead of 100%. All of the models eventually converge to very low estimation error, which shows that the EKF method is much more robust than others (Coulomb counting, for example, would never recover if incorrectly initialized). Eventual convergence is no great surprise with the EKF, however, as the cell voltage approaching 3.0 V will force the SOC estimate toward 0%. The best convergence results are seen with the higher fidelity cell models. The ESC model, in particular, shows fastest convergence, within only a few minutes, with most accurate error bounds. While an initialization error of 20% is an extreme condition, not expected in practice, the EKF is able to recover; this robustness is a very positive feature.

Not to belabor the discussion any further, we briefly report some results using EKF SOC estimation for the UDDS tests, shown in Fig. 6. Again, the ESC model performed best, so we only report results for that model, using four filter states. Frame (a) shows estimation error for correct initialization to 100% SOC, and frame (b) shows error when the EKF SOC state was incorrectly initialized to 80%. Estimation error is small, the confidence interval is reasonable, and convergence within a few minutes is observed even when poorly initialized.

Before we conclude our discussion of SOC estimation, it is necessary to emphasize that this method may be used to estimate the SOC of a *cell*. Multiple extended Kalman filters must be employed to estimate the states-of-charge of cells in a battery pack comprising a series string of cells; that is, the EKF does not directly estimate the SOC of a battery *pack*. In fact, the problem of finding pack SOC is ill-posed. If one cell has SOC equal to 0% and another has SOC equal to 100%, is the pack SOC equal to 50%? This would indicate that half of the rated pack capacity is available for charge or discharge, when in fact no charging or discharging may be done without taking one of these two cells outside of their design limits. If all cell SOCs are relatively similar, then "pack SOC" computed as an average or median value of cell SOCs might be somewhat useful to an HEV or BEV operator as a crude "gas gauge", but is not appropriate for computing available power, for example. We now present a better way to do so.

3. Application III: computing available power

State estimates and their uncertainties may be used to very accurately estimate how much power is available to be sourced or sunk by a battery pack while the pack is in a dynamic environment. This is described in some detail in [29], and summarized here.

The "Hybrid Pulse Power Characterization" (HPPC) method specified by the "Partnership for New Generation Vehicles" (PNGV) [30] is commonly used to calculate the available power from a cell during cell testing. Maximum current is computed using a simple cell model, enforcing that the cell's terminal voltage remains within limits, and power is computed by multiplying cell current by cell voltage. SOC is an input to this procedure, as are modified dis/charge resistances, found by cell tests.[2] Pack power is calculated by multiplying cell power by the number of cells in the pack.

By using an advanced cell model, such as the enhanced self-correcting cell model, together with the cell's present state vector estimated by EKF, we can achieve more accurate power estimates that depend on the cells' dynamic status. The battery pack cell models are simulated for Δt seconds into the future, using present states as identified by the EKF as the starting point, for some level of current i_k. A bisection search is used to find the maximum values of i_k for charge and discharge that do not cause any cell voltages or SOC

[2] The PNGV HPPC method uses modified resistances that model the relative voltage change for a 18-s prediction horizon on discharge or a 2-s prediction horizon on charge. The method presented here works for any horizon Δt.

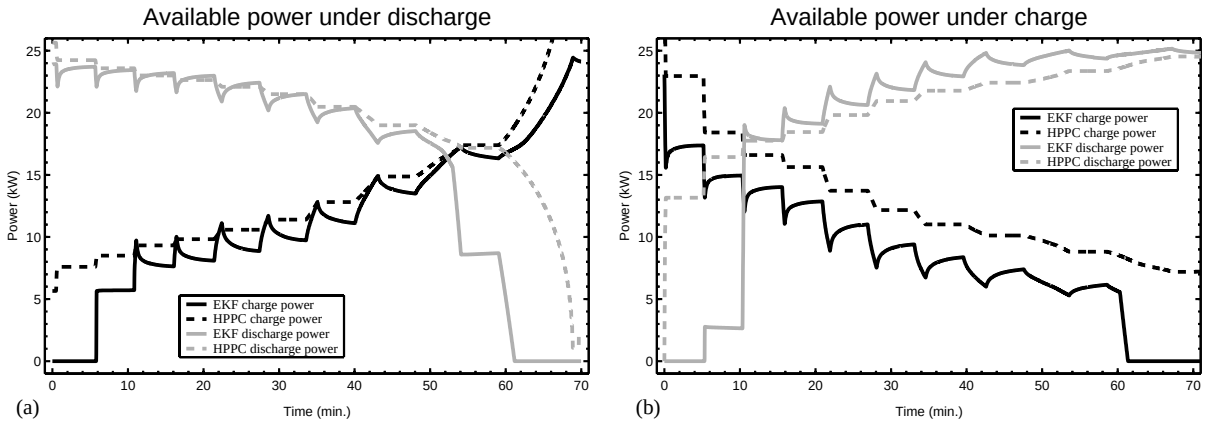

Fig. 7. Results of power estimation on pulsed-current data. Frame (a) shows the power estimates for the discharge portion of the test; Frame (b) shows the estimates for the charge portion of the tests.

values to violate design limits. Power is computed as the minimum of the maximum cell current limits, multiplied by cell voltage Δt seconds into the future.

Because this method uses all state information, more charging power is allowed immediately after a discharge event than after the cell has rested for some time, as the voltages will take more time to exceed design limits for the same current level. Similarly, immediately after a charge event, more discharge power will be available than after the cell has rested some time. Maximum power results for the pulsed-current test are shown in Fig. 7(a) for discharge and (b) for charge. (We assume a pack of 40 series-connected cells. Note that it is not our purpose here to comment on the absolute capability of these cells as compared to other cells, but rather on the merits of two power-calculation methods. The optimization of cell electrochemistry is the topic of other research.)

Over the discharge portion of the pulsed-current test we see fair agreement between the EKF-based power calculations and the HPPC estimate. The EKF method imposes the constraint that SOC is not allowed outside the range 10–90%, which explains why the permitted charge power is initially zero, until the cell SOC drops to below 90%, and why the discharge power drops to zero after about 60 min, when the cell SOC falls below 10%. Over the intermediate SOC range the results are "close", although we believe that the HPPC results are less accurate than the EKF results as the simple resistance model of a cell employed by HPPC is not very accurate. In particular, note that the EKF correctly allows greater charge power and lower discharge power during discharge pulses, converging to some constant value during rest periods as the cell relaxes. The HPPC method—which has no information regarding voltage-relaxation states—predicts a constant value for dis/charge power during rest periods, which may be overly optimistic or pessimistic, depending on recent cell history.

Over the charge portion of the pulsed-current test, shown in frame (b), we see less agreement between the two methods. The HPPC method does not take into account any model of hysteresis. In fact, during charge, the at-rest terminal voltage is always higher than during discharge at the same SOC level, so greater discharge power and less charge power should be available. The EKF method takes into account cell voltage hysteresis, and is able to more accurately predict cell available power.

4. Application IV: dual state and cell parameter estimation

Not all cells are created equal. Most of the research reported here has been conducted using prototype high-power LiPB cells, constructed by hand. In these cells, there is a great deal of variability in resistance, capacity, time constants, and so forth. Even in mass-produced cells, however, there is some cell-to-cell variation, which only increases as the cells age, both in accumulated cycles and in calendar life.

Some of the critical parameters, such as cell resistance and capacity, directly limit the pack performance through "power fade" and "capacity fade". The state-of-health (SOH) of a battery is often described using these values. It is important to be able to estimate these and other parameters to understand the present battery state-of-health, and to predict remaining service life.

Keeping in mind the previous discussion on estimating SOC, it is apparent that the quantities descriptive of the present battery pack condition exist on two time scales. Some change rapidly, such as SOC, which can traverse its entire range within minutes. Others may change very slowly, such as pack cell capacity, which might change as little as 20% in a decade or more of regular use. The quantities that tend to change quickly comprise the *state* of the system, and the quantities that tend to change slowly comprise the *time-varying parameters* of the system.

The method used to estimate SOC might be adapted to concurrently estimate both the state and the slowly time-varying cell parameters by augmenting the cell-model state vector with the model parameters and simultaneously

estimating the values of this augmented state vector. This method is called *joint estimation*. It has the disadvantage of large matrix operations due to the high dimensionality of the resulting augmented model. The method we describe here, *dual estimation*, also uses a Kalman filtering approach to estimate both state and parameter values, but uses separate Kalman filters for state estimation and parameter estimation. The matrix operations are simpler.

We slightly revise the mathematical model of cell dynamics to explicitly include the parameters

$$\begin{aligned} x_{k+1} &= f(x_k, u_k, \theta_k) + w_k \\ y_k &= g(x_k, u_k, \theta_k) + v_k, \end{aligned}$$

where x_k is the cell-model state, θ_k the set of time-varying model parameters, u_k the exogenous input, y_k the system output, and w_k and v_k are "noise inputs"; all quantities may be scalars or vectors. $f(\cdot,\cdot,\cdot)$ and $g(\cdot,\cdot,\cdot)$ are functions defined by the cell model being used. Non-time-varying numeric values required by the model may be embedded within $f(\cdot,\cdot,\cdot)$ and $g(\cdot,\cdot,\cdot)$, and are not included in θ_k.

To use the enhanced self-correcting cell model as an example, the possibly time-varying parameters comprise the following: the Coulombic efficiency η, the total capacity C, the filter poles $\alpha_1, \ldots, \alpha_{n_f}$, the filter weighting factors $g_1, \ldots, g_{n_f-1}$, the cell discharge and charge resistances R^+ and R^-, the hysteresis rate constant γ, and the maximum level of hysteresis M. Combined, they are

$$\theta = [\eta, C, \alpha_1, \ldots, \alpha_{n_f}, g_1, \ldots, g_{n_f-1}, R^+, R^-, \gamma, M]'.$$

We assume that there is a true value for θ that describes the cell under consideration, and wish to adapt an estimate $\hat{\theta}$ to converge to the true value. To do so using EKF we require a state-space model for the "dynamics" of the true parameters

$$\begin{aligned} \theta_{k+1} &= \theta_k + r_k \\ d_k &= g(x_k, u_k, \theta_k) + e_k. \end{aligned}$$

The first equation states that the parameters are essentially constant, but that they may change slowly over time by some driving process, modeled by a process r_k of small fictitious "noise". The output equation for the state-space model of true parameter dynamics is the cell output estimate plus some estimation error e_k.

With these two systems defined, we can apply the standard procedure of dual extended Kalman filtering [31]. The algorithm is outlined in Table 3 and comprises two carefully integrated EKFs. The algorithm is initialized by setting $\hat{\theta}$ to the best guess of the true parameters $\hat{\theta}_0^+ = \mathbb{E}[\theta_0]$, and by setting $\hat{x}_0^+$ to the best guess of the cell state $\hat{x}_0^+ = \mathbb{E}[x_0]$. The estimation error covariance matrices are also initialized.

Each measurement interval, several steps are performed. First, the previous parameter estimate is propagated forward in time. The new parameter estimate is equal to the old parameter estimate, and the parameter error uncertainty is increased due to the passage of time (as accommodated for in the model by the fictitious driving noise e_k). Next, the state estimate and its uncertainty are propagated forward one step in time. A measurement of the cell output is made, compared with the predicted output based on $\hat{x}_k^-$ and $\hat{\theta}_k^-$, and used to update the values of $\hat{x}$ and $\hat{\theta}$.

A subtle point relates to the computation of C_k^θ, which requires a total-differential expansion to be correct

$$\begin{aligned} C_k^\theta &= \left.\frac{\mathrm{d}g(\hat{x}_k^-, u_k, \theta)}{\mathrm{d}\theta}\right|_{\theta=\hat{\theta}_k^-} \\ \frac{\mathrm{d}g(\hat{x}_k^-, u_k, \theta)}{\mathrm{d}\theta} &= \frac{\partial g(\hat{x}_k^-, u_k, \theta)}{\partial \theta} + \frac{\partial g(\hat{x}_k^-, u_k, \theta)}{\partial \hat{x}_k^-}\frac{\mathrm{d}\hat{x}_k^-}{\mathrm{d}\theta} \\ \frac{\mathrm{d}\hat{x}_k^-}{\mathrm{d}\theta} &= \frac{\partial f(\hat{x}_{k-1}^+, u_{k-1}, \theta)}{\partial \theta} \\ &\quad + \frac{\partial f(\hat{x}_{k-1}^+, u_{k-1}, \theta)}{\partial \hat{x}_{k-1}^+}\frac{\mathrm{d}\hat{x}_{k-1}^+}{\mathrm{d}\theta}, \\ \frac{\mathrm{d}\hat{x}_{k-1}^+}{\mathrm{d}\theta} &= \frac{\mathrm{d}\hat{x}_{k-1}^-}{\mathrm{d}\theta} - L_{k-1}^x \frac{\mathrm{d}g(\hat{x}_{k-1}^-, u_{k-1}, \theta)}{\mathrm{d}\theta}, \end{aligned}$$

Table 3
Summary of the dual extended Kalman filter for state and parameter estimation [27]

Nonlinear state-space models[a]

$$x_{k+1} = f(x_k, u_k, \theta_k) + w_k,\ \theta_{k+1} = \theta_k + r_k$$

and

$$y_k = g(x_k, u_k, \theta_k) + v_k \qquad d_k = g(x_k, u_k, \theta_k) + e_k$$

Definitions

$$A_{k-1} = \left.\frac{\partial f(x_{k-1}, u_{k-1}, \hat{\theta}_k^-)}{\partial x_{k-1}}\right|_{x_{k-1}=\hat{x}_{k-1}^+}, \quad C_k^x = \left.\frac{\partial g(x_k, u_k, \hat{\theta}_k^-)}{\partial x_k}\right|_{x_k=\hat{x}_k^-},$$

$$C_k^\theta = \left.\frac{\mathrm{d}g(\hat{x}_k^-, u_k, \theta)}{\mathrm{d}\theta}\right|_{\theta=\hat{\theta}_k^-}$$

Initialization

For $k = 0$, set

$$\hat{\theta}_0^+ = \mathbb{E}[x_0], \quad \Sigma_{\tilde{\theta},0}^+ = \mathbb{E}[(\theta_0 - \hat{\theta}_0^+)(\theta_0 - \hat{\theta}_0^+)^{\mathrm{T}}]$$
$$\hat{x}_0^+ = \mathbb{E}[x_0], \quad \Sigma_{\tilde{x},0}^+ = \mathbb{E}[(x_0 - \hat{x}_0^+)(x_0 - \hat{x}_0^+)^{\mathrm{T}}]$$

Computation

For $k = 1, 2, \ldots$ compute

Time update for the weight filter

$$\hat{\theta}_k^- = \hat{\theta}_{k-1}^+$$
$$\Sigma_{\tilde{\theta},k}^- = \Sigma_{\tilde{\theta},k-1}^+ + \Sigma_r$$

Time update for the state filter

$$\hat{x}_k^- = f(\hat{x}_{k-1}^+, u_{k-1}, \hat{\theta}_k^-)$$
$$\Sigma_{\tilde{x},k}^- = A_{k-1}\Sigma_{\tilde{x},k-1}^+ A_{k-1}^{\mathrm{T}} + \Sigma_w$$

Measurement update for the state filter

$$L_k^x = \Sigma_{\tilde{x},k}^-(C_k^x)^{\mathrm{T}}[C_k^x\Sigma_{\tilde{x},k}^-(C_k^x)^{\mathrm{T}} + \Sigma_v]^{-1}$$
$$\hat{x}_k^+ = \hat{x}_k^- + L_k^x[y_k - g(\hat{x}_k^-, u_k, \hat{\theta}_k^-)]$$
$$\Sigma_{\tilde{x},k}^+ = (I - L_k^x C_k^x)\Sigma_{\tilde{x},k}^-$$

Measurement update for the weight filter

$$L_k^\theta = \Sigma_{\tilde{\theta},k}^-(C_k^\theta)^{\mathrm{T}}[C_k^\theta\Sigma_{\tilde{\theta},k}^-(C_k^\theta)^{T} + \Sigma_e]^{-1}$$
$$\hat{\theta}_k^+ = \hat{\theta}_k^- + L_k^\theta[y_k - g(\hat{x}_k^-, u_k, \hat{\theta}_k^-)]$$
$$\Sigma_{\tilde{\theta},k}^+ = (I - L_k^\theta C_k^\theta)\Sigma_{\tilde{\theta},k}^-$$

[a] w_k, v_k, r_k and e_k are independent, zero-mean, Gaussian noise processes of covariance matrices Σ_w, Σ_v, Σ_r and Σ_e, respectively.

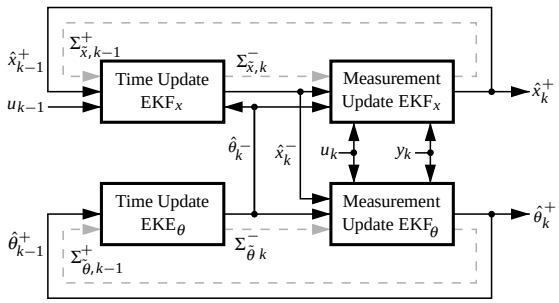

Fig. 8. Diagram of dual estimation method. Solid lines represent state and parameter vector signal flow, and dashed gray lines represent error covariance matrix signal flow.

assuming that L^x_{k-1} is not a function of θ. (Its is, weakly, so that it is not usually worth the extra computation to include the effects of L^x_{k-1} as a function of θ.) The three total derivatives are computed recursively, initialized on key-on with zero values. The partial derivatives are computed each time step, given knowledge of the specific $f(\cdot,\cdot,\cdot)$ and $g(\cdot,\cdot,\cdot)$ from the cell model being used.

The dual extended Kalman filter can be viewed by drawing a block diagram as in Fig. 8. We see that the process essentially comprises two extended Kalman filters running in parallel—one adapting the state and one adapting parameters—with some information exchange between the filters.

4.1. Ensuring correct convergence

The dual extended Kalman filter will adapt $\hat{x}$ and $\hat{\theta}$ so that the model input–output relationship matches the cell input–output data as closely as possible. There is no built-in guarantee that the state of the model converges to anything with physical meaning. Here, we are concerned that the state converge to a very specific meaning. That is, assuming the enhanced self-correcting cell model, we require some state values to be filter voltages, one to be hysteresis level, and one to be SOC. We take special steps to ensure that this occurs.

First, a very crude cell model may be used, combined with the dual EKF to ensure convergence of the SOC state. Specifically, the cell terminal voltage

$$\begin{aligned} v_k &\approx \mathrm{OCV}(z_k) - Ri_k \\ \mathrm{OCV}(z_k) &\approx v_k + Ri_k \\ \hat{z}_k &= \mathrm{OCV}^{-1}(v_k + Ri_k). \end{aligned}$$

By measuring the cell voltage under load, v_k, the cell current i_k, and having knowledge of R (perhaps through $\hat{\theta}$ from the dual EKF), and knowing the inverse OCV function for the cell chemistry, one can compute a noisy estimate of SOC, $\hat{z}_k$.

The cell model being used for dual EKF has its output equation augmented with SOC. For example,

$$g(x_k, u_k, \theta) = \begin{bmatrix} \mathrm{OCV}(z_k) - Ri_k + Mh_k + Gf_k \\ z_k \end{bmatrix}.$$

The dual EKF is run using this modified model with the "measured" information used in the measurement update being

$$y_k = \begin{bmatrix} v_k \\ \hat{z}_k \end{bmatrix}.$$

While the "noise" of $\hat{z}_k$ (short-term bias due to hysteresis effects and polarization filter voltages being ignored) prohibit it from being used as the primary estimator of SOC, its expected long-term behavior in a dynamic environment is accurate, and maintains the accuracy of the SOC state in the dual EKF.

Convergence of the hysteresis state and voltage polarization states to the true values may be indirectly ensured if the cell model has been carefully crafted. For example, consider the output equation of the enhanced self-correcting cell model:

$$g(x_k, u_k) = \underbrace{\mathrm{OCV}(z_k)}_{\mathrm{fn}(z_k)} + \underbrace{h_k}_{\mathrm{fn}(z_k, i_k)} + \underbrace{\mathrm{filt}(i_k) - Ri_k}_{\mathrm{fn}(i_k)}.$$

The filter $\mathrm{filt}(i_k)$ is designed to have zero dc gain, so a dc bias can only be accounted for by $\mathrm{OCV}(z_k)$, whose convergence has already been ensured, and h_k. For the model rest voltage to match the cell rest voltage, the hysteresis value is forced to converge to the actual level. The dc value during a constant-current dis/charge adds another term—the R value in Ri_k, forcing R to converge. Finally, fluctuations around the dc value due to dynamic current events are only accommodated for by the poles and weighting factors of the filter Gf_k. The filter time constants, related to $\alpha_1, \ldots, \alpha_{n_f}$, must converge due to the near stationarity of cell dynamics, and the weighting values G only determine the gains of the f_k states.

4.2. Methods for estimating SOH without the full dual EKF

The full dual EKF method is computationally intensive. If precise values for the full set of cell-model parameters are not necessary, then other methods might be used. Here, we present methods to determine cell capacity and resistance using EKF-based methods. The change in capacity and resistance from the nominal "new-cell" values give capacity fade and power fade, which are the most commonly employed indicators of cell SOH.

4.2.1. Estimating resistance

To estimate cell resistance using an EKF mechanism, we formulate a simple model

$$\begin{aligned} R_{k+1} &= R_k + r_k \\ y_k &= \mathrm{OCV}(z_k) - R_k i_k + e_k, \end{aligned}$$

where R_k is the cell resistance and is modeled as a constant value with a fictitious noise process r_k allowing adaptation.

y_k is a crude estimate of the cell's voltage, i_k is the cell current, and e_k models estimation error. If we use an estimate of z_k from the state EKF, or from some other source, we simply apply an EKF to this model to estimate cell resistance. In the standard EKF, we compute the model's prediction of y_k with the true measured cell voltage, and use the difference to adapt R_k.

Note that the above model may be extended to handle different values of resistance on charge and discharge, different values of resistance at different SOCs, and different values of resistance at different temperatures, for example. The scalar R_k would be changed into a vector comprising all of the resistance values being modified, and the appropriate element from the vector would be used each time step of the EKF during the calculations.

4.2.2. Estimating capacity

To estimate cell capacity using an EKF, we again formulate a simple cell model

$$C_{k+1} = C_k + r_k$$
$$d_k = z_k - z_{k-1} + \frac{\eta_i i_{k-1} \Delta t}{C_{k-1}} + e_k.$$

The second equation is a reformulation of the SOC state equation such that the expected value of d_k is equal to zero by construction. Again, an EKF is constructed using the model defined by these two equations to produce a capacity estimate. As the EKF runs, the computation for d_k in the second equation is compared to the known value (zero, by construction), and the difference is used to update the capacity estimate. Note that good estimates of the present and previous states-of-charge are required, possibly from an EKF estimating SOC. Estimated capacity may again be a function of temperature (and so forth), if desired, by employing a capacity vector, from which the appropriate element is used in each time step of the EKF during calculations.

4.3. Results of dual EKF

We now present several results to demonstrate features of the dual EKF algorithm. The first two results are "steady-state" estimates of resistance and capacity produced directly by the dual EKF algorithm. The second two results are from the auxiliary filters described in Sections 4.2.1 and 4.2.2.

Fig. 9 shows some results from dual estimation. In frame (a), we see the steady-state capacity estimate produced directly by the dual EKF. It has converged to the correct value, and exhibits little variation over time. In frame (b), we see the "steady-state" charge and discharge resistances produced directly by the dual EKF. We see that these estimates do

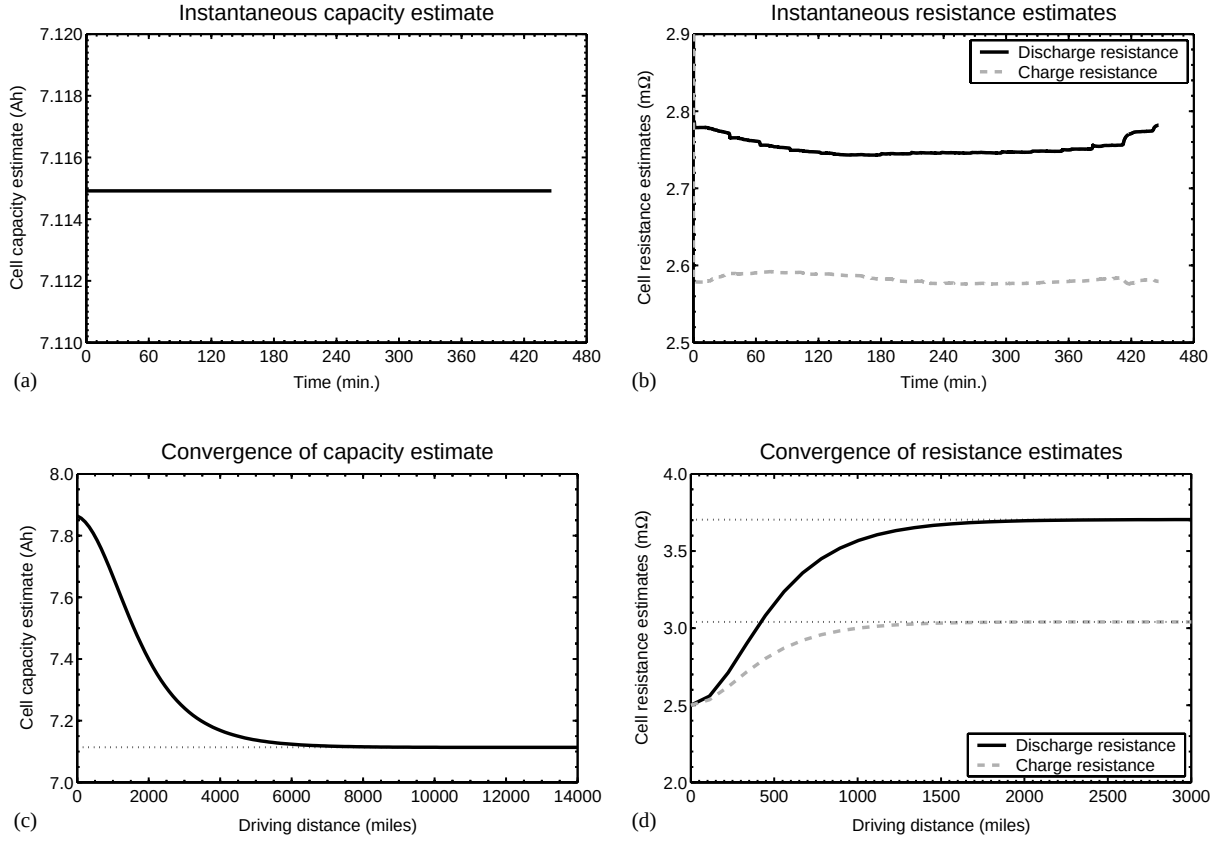

Fig. 9. Plots showing results of dual estimation. Frame (a) plots the "steady-state" capacity estimate and (b) plots the "steady-state" resistance estimate. Frame (c) plots the transient behavior of the capacity estimate and frame (d) plots the transient behavior of the resistance estimate.

not converge to a constant, but vary according to the present state-of-charge. As is expected for this chemistry, the (discharge) resistance is highest at high and low SOCs, and is lowest at moderate SOCs. The quickly varying nature of the dis/charge resistance estimates allows slightly better SOC estimation using dual EKF than using standard EKF with fixed resistance values.

If the complexity of the dual EKF is not warranted by an application, the simple filters from Sections 4.2.1 and 4.2.2 may be used. Results using these methods are plotted in Fig. 9(c) and (d). In frame (c), the state of the auxiliary capacity estimation filter was initially set about 10% too high and adaptation was allowed to occur. In frame (d) the states of the auxiliary resistance estimation filter were set significantly too low, and adaptation was allowed to occur. In both cases, the estimates converge to the correct values.[3] The horizontal axis for the plots was determined by noting that a UDDS cycle covers 7.45 miles, and that the UDDS test has 15 such cycles in it. Many repetitions of the UDDS test were required for parameter convergence.

Is convergence fast enough? If we consider that the capacity of an HEV cell must degrade less than 20% over a vehicle lifetime (say, 150,000 miles), then the time constant of capacity change is in the order of 50,000 miles. For an estimator to track a moving target, its time constant must be at least four times faster than that of the moving target (faster is better). Here, we see that the capacity filter time constant is in the order of 2000 miles, and the resistance filter time constant is in the order of 500 miles. Both filters are faster than they need be. Note that this example is extreme; in an application the HEV cells would be mass produced with high quality control and tight tolerances on initial capacity and resistance. The filters would then be initialized with accurate values, and are fast enough to track changes. In fact, the filters can be "tuned" by varying the values for Σ_r and Σ_e to be either faster or slower than those shown. Faster filters do converge more quickly, but produce noisier steady-state estimates. Slower filters produce cleaner steady-state estimates. The tuning of the filter must be done to meet design specifications.

5. Application V: equalization via SOC

Over time, cells in a battery pack (comprising a series-connected string of cells) may become "out of balance" as small differences in their dynamics—principally, in their Coulombic efficiencies and capacities—cause their states of charge to drift apart from each other. The danger is that one or more cells may eventually limit the discharge ability of the pack if their SOC is much lower than that of the others, and one or more cells may limit the charging capacity of the pack if their SOC is much higher than that of the others. In an extreme case, the pack can neither be discharged nor charged if one cell is at the low SOC limit and another is at the high SOC limit, even if all other cells are at intermediate values. Packs may be *balanced* or *equalized* by "boosting" (individually adding charge to) cells with SOC too low, "bucking" (individually depleting charge from) cells with SOC too high or "shuffling" (moving charge from one cell to another).

In HEV, determining which cells must have their charge levels adjusted to equalize the pack is generally done on the basis of cell voltage alone. The pack is considered to be properly balanced if all cell voltages are the same, perhaps within some tolerance. Various electronic means are available to perform the equalization, either automatically, or under microprocessor control. These include: shuffling charge using a switched capacitor, depleting charge with a resistor, adding charge with a DC–DC converter, or moving charge with a transformer-based system. These methods are very well described in [32].

With the information available from a dual EKF, for example, another opportunity presents itself. We propose that equalizing cell voltage is only approximately the correct thing to do. Recall that the purpose of equalization is to maintain the battery pack in a state where the maximum level of charge and discharge power is available for use. Cells that limit the pack availability may then be boosted or bucked in order to improve performance. These cells might be determined in at least two ways. First, one might use side-information from the maximum power calculation stating which cells caused the available power to be limited. If using the method from Section 3, then this determination would consider cells by voltage limit and by SOC limit. The second way more simply considers potential SOC limits. Here, we investigate this approach.

Consider a pack with operational design limits such that every cell SOC $z_k(t)$ must reside in the range $z_{\min} \leq z_k(t) \leq z_{\max}$. For SOC of cell k at level $z_k(t)$, the "distance" in ampere-hours from the upper limit is

$$C_k^{\text{charge}}(t) = (z_{\max} - z_k(t))C_k$$

and the distance in ampere-hours from the lower limit is

$$C_k^{\text{discharge}}(t) = (z_k(t) - z_{\min})C_k,$$

where C_k is the capacity of cell k, in ampere-hours. If all cells have equal $C_k^{\text{charge}}(t)$, then no cell will limit pack charge capacity. However, if the capacity of one cell is lower than that of others, it will limit the ability of the pack to accept charge. Similarly, if all cells have equal $C_k^{\text{discharge}}(t)$, then no cell will limit pack discharge capacity. If one capacity is

[3] The resistance values in frame (b) differ from those in frame (d) because the ESC model used in the simulations in frame (b) has a separate hysteresis term and so the resistance states are adapted to their true values. The crude cell model used in the simulations of fame (d) have no such hysteresis correction factor, so the resistances attempt to capture the ohmic behavior as well as the hysteretic behavior of the cell dynamics. This results in larger-than-true values for resistance, which may be taken into account in an implementation.

lower than the others, it will limit the ability of the pack to supply charge.

We can use this information to derive a simple procedure to determine which cells require equalization:

1. Compute $C_k^{\text{discharge}}$ for all cells, and sort from smallest to largest. The cells with smallest value may benefit from having some charge depleted via bucking, prioritized by the magnitude of its $C_k^{\text{discharge}}$.
2. Compute C_k^{charge} for all cells, and sort from smallest to largest. The cells with smallest value may benefit from having charge added via boosting, prioritized by the magnitude of its C_k^{charge}.
3. If charge shuffling is available, it should be shuffled from the cell with minimum C_k^{charge} to the one with minimum $C_k^{\text{discharge}}$.

The EKF used to estimate SOC may also contribute the estimation error bounds to help determine when to stop equalization. For example, one might turn off equalization if the difference between maximum and minimum $C_k^{\text{discharge}}$ and the difference between maximum and minimum C_k^{charge} falls within $3\sigma C_{\text{n}}$. Also, if the same cell is targeted for both boosting and bucking, it is the cell limiting performance whether or not its SOC is changed, so equalization may be turned off.

If cell capacity information is not individually available, then the nominal capacity C_{n} may be used. If so, the procedure then equalizes SOC, which is not exactly the same as equalizing cell voltage. If all cell dynamic characteristics are equal, then the method becomes the same as equalizing by voltage. We expect that as cells in a battery pack age, their characteristics will not remain equal, so that by using the proposed method here the pack will provide better performance in the long run.

6. Conclusions

In this series of three papers, we have described how extended Kalman filtering might be used by a battery management system in some of its key algorithmic roles. In this paper, we have looked at the applications of the theory and cell models presented in the earlier two.

First, we showed how an EKF might be used during key-on initialization, to update cell SOC estimates saved on key-off, to account for cell self-discharge during the key-off interval. A very simple self-discharge model is used together with a single step of the EKF.

Secondly, we showed how an EKF might be used, together with a model of cell dynamics, to dynamically estimate SOC and other state vector values. Additionally, error bounds on the estimate are generated. Robust behavior, even when poorly initialized, is observed. SOC estimation error within a few percent is typical.

An argument against using EKF for SOC estimation is that it appears very complex to implement. Instead, one might wish to use a simpler method; for example, Coulomb counting. However, estimation error accumulates when integrating ampere-hours, and is guaranteed to eventually diverge. Even in short tests of several hours duration with state-of-the-art battery test equipment (an Aerovironment ABC-150), we have observed occasions where the EKF SOC estimate (using much poorer and less expensive sensors) is more accurate than the ABC-150 ampere-hour integration. One might add correction factors to a simple method to perform voltage versus SOC correction. However, the discharge curve for our cells is very flat, so there is very little information in a voltage measurement alone. Other correction factors must be added for temperature, cell aging, and so forth. In the end, the “simple” method boils down to a spaghetti-heap of correction factors and special cases. The EKF, however, is an extension of the optimal recursive estimation method first developed by Kalman in 1960 [33,34]. Its extensive use in other applications (e.g., defense, control, navigation, space, etc.) and its kinship with other DSP applications has ensured the development of microprocessors that are capable of implementing the required multiply and accumulate operations quickly and efficiently. In short, we feel that the EKF provides the best solution for the long term.

The third application presented in this paper uses the state estimate provided by the EKF to give dynamic available power estimates. These estimates automatically compensate for recent dis/charge events, which have brought cell voltage out of equilibrium and give a more precise estimate of how much power may be drawn without exceeding voltage limits. Methods that do not use this information, such as the PNGV HPPC method, either give estimates that are too conservative or too risky.

The fourth application integrates two nearly independent extended Kalman filters in order to simultaneously estimate state and cell-model parameter values. This is very valuable for keeping the other EKFs “honest” over the lifetime of the battery pack as cells age and their characteristics change. This has the important benefit of extending the useful service life during which the pack may be safely and reliably operated. Estimates of SOH are also generated by the direct estimation of cell resistance (power fade) and capacity (capacity fade).

The fifth, and final, application is to use information from the dual EKF to enhance the selection of cells that require equalization. Voltage-based equalization only approximately implements the best strategy. If hardware is available to individually select cells for equalization, the SOC-based strategy presented here will work better, especially as the pack ages and cell capacities diverge.

We have tested these methods using data collected from hand-made prototype LiPB cells jointly developed by LG Chem (Daejeon, Korea) and Compact Power Inc. (Monument, Colorado). Furthermore, to date we have implemented a large subset of the algorithms on a prototype BMS

developed by Compact Power Inc. for HEV application. We find that even with hand-made cells the full implementation provides similar performance to the cell-by-cell results. For example, SOC estimation error is rarely greater than 5% over operating conditions between 0 and 50 °C for all types of tests. We expect that performance will improve with mass-produced cells which will have more homogeneous characteristics. Future research will focus on improving low-temperature performance.

In conclusion, EKF methods are a good approach to fulfilling the algorithmic requirements of an HEV BMS.

Acknowledgements

This work was supported in part by Compact Power Inc. (CPI). The use of company facilities, and many enlightening discussions with Drs. Mohamed Alamgir and Dan Rivers and others are gratefully acknowledged.

References

[1] G. Plett, Extended Kalman filtering for battery management systems of LiPB-based HEV battery packs, Part 1, Background, J. Power Sour. 134 (2) (2004) 252–261.
[2] G. Plett, Extended Kalman filtering for battery management systems of LiPB-based HEV battery packs, Part 2, Modeling and identification, J. Power Sour. 134 (2) (2004) 262–276.
[3] A. Clegg, Current state-of-health [battery monitoring], Commun. Int. 19 (7) (1992) 39–41.
[4] D. Baert, A. Vervaet, Determination of the state-of-health of vrla batteries by means of noise measurements, in: Proceedings of the 23rd International Telecommunications Energy Conference, INTELEC 2001, IEE, London, UK, 2001, pp. 301–306.
[5] M. Ignatov, B. Monahov, Some problems of assessing the state-of-health of lead-acid batteries during operation, in: Proceedings of the First International Telecommunications Energy Conference, VDE, Frankfurt/Main, Germany, 1994, pp. 105–111.
[6] A. Green, Investigations into methods of measuring the state-of-health of a nickel–cadmium industrial battery, in: Standby Batteries; Balancing Reliability and Monitoring with Costs. Conference Volume, ERA Technol., Leatherhead, UK, 1998, pp. 2.3.1–2.3.7.
[7] C. Bose, F. Laman, Battery state-of-health estimation through coup de fouet, in: Proceedings of the International IEEE Telecommunications Energy Conference, IEEE Power Electronics Society, IEEE, Piscataway, NJ, 2000, pp. 597–601.
[8] C. Bose, D. Wilkins, S. McCluer, M. Model, Lessons learned in using ohmic techniques for battery monitoring, in: Proceedings of the 16th Annual Battery Conference on Applications and Advances, IEEE, Piscataway, NJ, 2001, pp. 99–104.
[9] D. Feder, T. Croda, K. Champlin, S. McShane, M. Hlavac, Conductance testing compared to traditional methods of evaluating the capacity of valve-regulated lead/acid batteries and predicting state-of-health, J. Power Sour. 40 (1–2) (1992) 235–250.
[10] D. Feder, T. Croda, K. Champlin, M. Hlavac, Field and laboratory studies to assess the state-of-health of valve-regulated lead acid batteries, I, Conductance/capacity correlation studies, in: Proceedings of the 14th International Telecommunications Energy Conference, INTELEC'92, IEEE, New York, NY, 1992, pp. 218–233.
[11] D. Feder, M. Hlavac, W. Koster, Evaluating the state-of-health of flooded and valve-regulated lead/acid batteries: a comparison of conductance testing with traditional methods, J. Power Sour. 46 (2–3) (1993) 391–415.
[12] D. Feder, M. Hlavac, Analysis and interpretation of conductance measurements used to assess the state-of-health of valve regulated lead acid batteries, in: Proceedings of the 16th International Telecommunications Energy Conference, INTELEC'94, IEEE, New York, NY, 1994, pp. 282–291.
[13] D. Feder, M. Hlavac, S. McShane, Updated status of conductance/capacity correlation studies to determine the state-of-health of automotive and stand-by lead/acid batteries, J. Power Sour. 48 (1–2) (1994) 135–161.
[14] A. Waters, K. Bullock, C. Bose, Monitoring the state-of-health of vrla batteries through ohmic measurements, in: Proceedings of the 19th International Telecommunications Energy Conference, INTELEC'97, IEEE, New York, NY, 1997, pp. 675–680.
[15] F. Huet, A review of impedance measurements for determination of the state-of-charge or state-of-health of secondary batteries, J. Power Sour. 70 (1998) 59–69.
[16] P. Singh, D. Reisner, Fuzzy logic-based state-of-health determination of lead acid batteries, in: Proceedings of the International Telecommunications Energy Conference, INTELEC 2002, IEEE, Piscataway, NJ, 2002, pp. 583–590.
[17] I. Damlund, Analysis and interpretation of ac-measurements on batteries used to assess state-of-health and capacity-condition, in: Proceedings of the 17th International Telecommunications Energy Conference, INTELEC'95, IEEE, New York, NY, 1995, pp. 828–833.
[18] M. Hlavac, D. Feder, T. Croda, K. Champlin, Field and laboratory studies to assess the state-of-health of valve-regulated lead acid and other battery technologies using conductance testing, in: Proceedings of the 15th International Telecommunications Energy Conference, INTELEC'93, vol. 2, IEEE, New York, NY, 1993, pp. 375–383.
[19] M. Hlavac, Field application of conductance measurements used to ascertain cell/battery and inter-cell connection state-of-health in electric power utility applications, in: Proceedings of the American Power Conference, Illinois Inst. Technol., vol. 1, Chicago, IL, 1993, pp. 44–57.
[20] I. Buchmann, Artificial intelligence reads battery state-of-health in three minutes, in: Proceedings of the 16th Annual Battery Conference on Applications and Advances, IEEE, Piscataway, NJ, 2001, pp. 263–265.
[21] R. Robinson, On-line battery testing: a reliable method for determining battery health? in: Proceedings of the INTELEC'96 International Telecommunications Energy Conference, IEEE Power Electronics Society, IEEE, New York, NY, 1996, pp. 654–661.
[22] D. Cox, R. Perez-Kite, Battery state-of-health monitoring, combining conductance technology with other measurement parameters for real-time battery performance analysis, in: Proceedings of the International IEEE Telecommunications Energy Conference, IEEE Power Electronics Society, IEEE, Piscataway, NJ, 2000, pp. 342–347.
[23] E. Meissner, G. Richter, Vehicle electric power systems are under change! Implications for design, monitoring and management of automotive batteries, J. Power Sour. 95 (2001) 13–23.
[24] T. Suntio, Imperfectness as a useful approach in battery monitoring, in: Proceedings of the 16th International Telecommunications Energy Conference, INTELEC'94, IEEE, New York, NY, 1994, pp. 481–485.
[25] V. Spath, A. Jossen, H. Doring, J. Garche, The detection of the state-of-health of lead-acid batteries, in: Proceedings of the 19th International Telecommunications Energy Conference, INTELEC'97, IEEE, New York, NY, 1997, pp. 681–686.
[26] A. Anbuky, P. Pascoe, P. Hunter, Knowledge based VRLA battery monitoring and health assessment, in: Proceedings of the International IEEE Telecommunications Energy Conference, IEEE Power Electronics Society, IEEE, Piscataway, NJ, 2000, pp. 687–694.
[27] E. Wan, A. Nelson, Dual extended Kalman filter methods, in: S. Haykin (Ed.), Kalman Filtering and Neural Networks, Wiley/InterScience, New York, 2001, pp. 123–174.

[28] CTTS Vehicle Systems Analysis Homepage, accessed on May 2003. http://www.ctts.nrel.gov/analysis/.
[29] G. Plett, High-performance battery-pack power estimation using a dynamic cell model, IEEE Trans. Veh. Technol., submitted for publication.
[30] U.S. Dept of Energy, Idaho National Engineering and Environmental Laboratory, PNGV Battery Test Manual, Revision 3, DOE/ID–10597, 2001.
[31] S. Haykin, Kalman Filtering and Neural Networks, Wiley/InterScience, New York, 2001.
[32] S. Moore, P. Schneider, A review of cell equalization methods for lithium ion and lithium polymer battery systems, in: Proceedings of the SAE 2001 World Congress, Advanced Hybrid Vehicle Powertrains, SAE, Warrendale, PA, Detroit, MI, 2001, 2001-01-0959.
[33] R. Kalman, A new approach to linear filtering and prediction problems, Trans. ASME, J. Basic Eng., Ser. D 82 (1960) 35–45.
[34] The Seminal Kalman Filter Paper, 1960, accessed on 20 May 2003. http://www.cs.unc.edu/∼welch/kalman/kalmanPaper.html.